Characteristics and control of Type I ELM in JT-60U

N. Oyama 1), N. Hayashi 1), N. Aiba 1), A. Isayama 1), H. Urano 1), Y. Sakamoto 1), Y. Kamada 1), T. Takizuka 1) and the JT-60 Team 1)

1) Japan Atomic Energy Agency, Naka, Ibaraki-ken, 311-0193 Japan

E-mail contact of main author: oyama.naoyuki@jaea.go.jp

Abstract. The detailed characteristics of the precursor of type I ELM have been studied in JT-60U using diagnostics with high temporal and spatial resolution such as microwave reflectometer, electron cyclotron emission (ECE) heterodyne radiometer and grating polychromator. Coherent density and temperature precursors have been observed before the collapse phase of the type I ELM. The growth rate of the precursor is evaluated to be $\gamma/\omega_A \sim 10^{-3}$ for several edge pedestal conditions. From the phase delay between ECE signals measured at two toroidal locations and the frequency of the precursor, the toroidal mode number is experimentally evaluated as n = 8-10 or 14-16 assuming that the precursor rotates toroidally with the same toroidal rotation speed of carbon impurity. It is found that the dominant n varies with each ELM under the same plasma condition. A new parameter of the ratio of the pressure gradient inside the pedestal (p'_{in}) to the pressure gradient within the pedestal (p'_{ped}) has been confirmed as an important parameter determining the ELM energy loss (ΔW_{ELM}) normalized to the pedestal stored energy (W_{ped}), $\Delta W_{ELM}/W_{ped}$. When the ratio of p'_{in}/p'_{ped} increases from 0.3 to 0.6, $\Delta W_{ELM}/W_{ped}$ increases from 0.04 to 0.10. The dependence can not be explained by either the edge collisionality dependence or the edge toroidal rotation dependence of $\Delta W_{ELM}/W_{ped}$. When the plasma near the top of the pedestal on the high-field side is heated by the electron cyclotron wave (ECW) power of 1.57 MW, the $\Delta W_{ELM}/W_{ped}$ was reduced by 33 %, together with the increase in the ELM frequency. The increasing rate of the ELM frequency with the heating power is four times larger in the ECW injection case than the neutral beam injection case, suggesting the localized ECW injection to the edge plasma can be considered as a candidate for an active ELM control technique in ITER.

1. Introduction

The rapid release of heat and particles from edge plasma due to edge localized modes (ELMs) is one of the critical issues in ITER, since the instantaneous heat load may determine the lifetime of plasma facing components and/or divertor targets. In Q = 10 inductive operation scenario for ITER, the high confinement mode (H-mode) plasma with type I ELMs has been considered as a reference scenario. However, the heat load limit of 0.5 MJ·m^{-2} for both of the tile materials, carbon and tungsten, requires an acceptable ELM energy loss (ΔW_{ELM}) of less than 1 MJ [1], which corresponds to about 1% of the pedestal stored energy (W_{ped}) in ITER. The current acceptable value relies on the normalized ELM energy loss of $\Delta W_{ELM}/W_{ped} \sim 0.2$ based only on the edge collisionality (ν_e^*) dependence of $\Delta W_{ELM}/W_{ped}$ [2]. Since other dependences have been observed as described below, better understanding of ELM physics and developing models of energy loss process due to ELMs with predictive capability are important for reliable prediction of the ELM energy loss in ITER. In parallel with these studies, investigations of small or no ELM regimes, and developments of active ELM control methods have been performed in many devices to establish ELM mitigation technique compatible with ITER reference scenario [3-5 and references therein].

In JT-60U, fast dynamics of type I ELMs has been investigated for developing a model of ELM [6]. In the previous experiments, however, the toroidal mode number of ELM precursors has not been evaluated using the magnetic probe array, since ELM precursors in magnetic fluctuation have not been observed. Thus, a new transmission line for electron cyclotron emission (ECE) diagnostics toroidally separated by 60 degrees from the original transmission line has been installed for the correlation analysis of temperature precursors in

JT-60U. Then, detailed characteristics of ELM precursor such as growth rate and mode number have been evaluated for understanding what kind of instability triggers the type I ELM. Prediction of the ELM energy loss in ITER is essentially important for evaluation of required conditions of ELM mitigation in ITER. The ν_e^* dependence has often been used for this purpose. However, a large variation of $\Delta W_{ELM}/W_{ped}$ has been observed in many tokamaks and so that other plasma parameters determining $\Delta W_{ELM}/W_{ped}$ have been proposed such as normalized ion gyroradius ($\rho^* = \rho/a$) in DIII-D [7] and edge toroidal rotation velocity (V_T) in JT-60U [8]. In addition to these parameters, the integrated simulation of ELM energy loss using TOPICS-IB code predicts the ratio of the pressure gradient inside the pedestal (p'_{in}) to the pressure gradient within the pedestal (p'_{ped}) can change $\Delta W_{ELM}/W_{ped}$ through the different radial profile of the eigenfunction of unstable modes [9]. To confirm the prediction, the dependence of $\Delta W_{ELM}/W_{ped}$ on p'_{in}/p'_{ped} predicted by TOPICS-IB code has been checked using experimental data in JT-60U. Active ELM control methods using resonant magnetic perturbation produced by internal coils and pellet injection have been considered as primary methods for ITER [4 and references therein]. Since there are still some remaining issues on these methods, alternative ELM mitigation techniques have been investigated. As one of them, modulated edge ECCD/ECH was applied in ASDEX Upgrade and the ELM frequency was clamped from ~150 Hz to the modulation frequency of 100 Hz [10]. In JT-60U, on the other hand, the effects of the continuous injection of the electron cyclotron wave (ECW) on $\Delta W_{ELM}/W_{ped}$ have been investigated.

2. Characteristics of type I ELM precursor

Coherent density and temperature precursors of type I ELMs are typically observed 200-500 μs before the collapse of the pedestal structure and the temperature precursor is observed within the narrow radial region at the pedestal [6]. In plasma with I_p = 1.6 MA and B_T = 4.0 T, simultaneous ELM precursor measurements are performed using the microwave reflectometer and the ECE radiometer, which measure the midplane plasma on the low-field side as shown in FIG. 1(a). A coherent density precursor is also observed in the line-integrated density using the vertical interferometer (FIR2) as shown in FIG. 1(c). In FIR1 signal measured at the high-field side, on the other hand, the amplitude of density fluctuation is about 10 % of that in FIR2 signal even if the viewing chord of FIR1 is passing through only the edge plasma region, $r/a > 0.7$, indicating that the ELM precursor is localized on a low field side, like a ballooning mode.

As shown in FIG. 1(d), the precursor in the density fluctuation measured with the reflectometer is most visible. The variation in the phase signal of the reflectometer is mainly attributed to the radial displacement of the cut-off density layer. As shown in the small box in FIG. 2, the growth of the amplitude of the density fluctuation can be fitted by an exponential function. In order to evaluate the growth rate (γ) of the precursor experimentally, the time constant of fitting curves is analyzed systematically using plasmas with I_p = 1.5 MA and B_T = 3.3 or 3.7 T. Then, the histogram of the time constant in three different pedestal conditions in terms of the pedestal stability such as the safety factor (edge current density) and/or the edge pressure are compared in FIG. 2. The distribution of the time constant has a peak near 150-200 μs and the shape of the histogram is similar in all three cases. Since the Alfvén frequencies (ω_A) of these plasmas are in the range of $4.7\text{-}4.9\times10^6$ rad·s^{-1}, the growth rate of the precursor normalized to ω_A is evaluated to be $\gamma/\omega_A \sim 10^{-3}$.

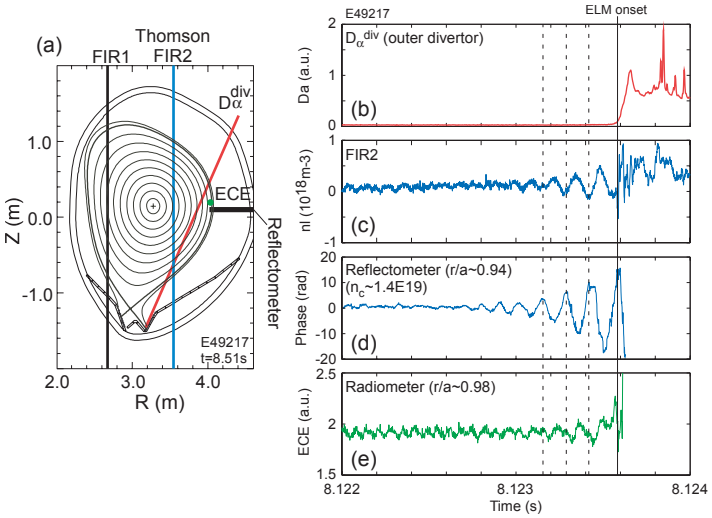

FIG. 1. (a) Plasma configuration for ELM precursor measurement together with the line of sight of two FIR interferometers, D_α intensity, reflectometer and measured location of ECE radiometer. Waveforms of (b) D_α intensity at outer divertor, (c) line-integrated density, (d) phase change of reflectometer signal and (e) ECE intensity of radiometer.

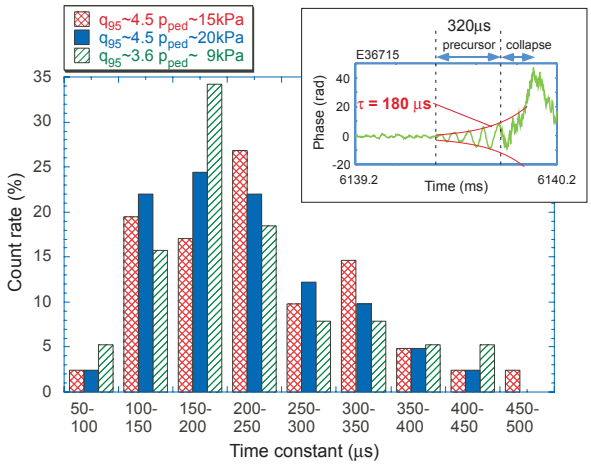

FIG. 2. Histogram of the time constant of amplitude of ELM precursor in the density fluctuation. Evolution of type I ELM precursor measured with reflectometer and an example of fitting line to determine the time constant are also shown in small box.

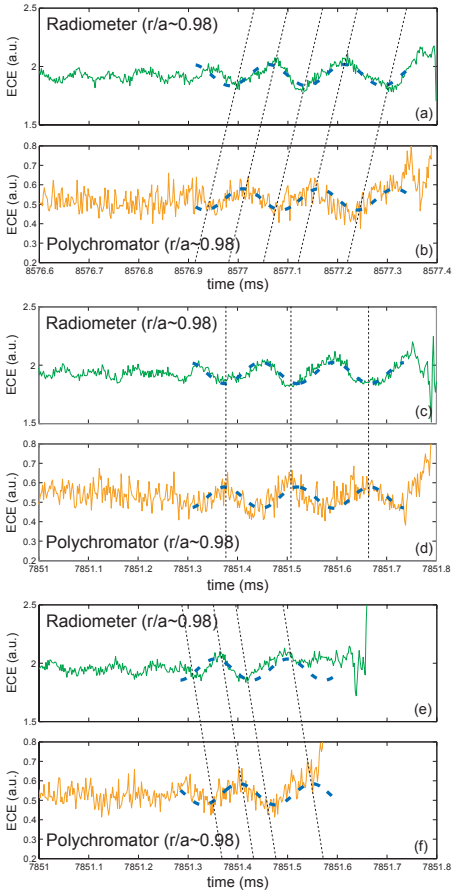

FIG. 3. Precursor signal in temperature fluctuations measured with (a), (c), (e) heterodyne radiometer and (b), (d), (f) grating polychromator in three cases. Dashed lines are simulated signal using model parameters of toroidal mode number and toroidal rotation speed.
(a)&(b): $n = 8$ ($V_T = -21.5$ km·s^{-1}) or $n = 14$ ($V_T = -12.3$ km·s^{-1}).
(c)&(d): $n = 9$ ($V_T = -20.0$ km·s^{-1}) or $n = 15$ ($V_T = -12.0$ km·s^{-1}).
(e)&(f): $n = 10$ ($V_T = -18.0$ km·s^{-1}) or $n = 16$ ($V_T = -11.3$ km·s^{-1}).
Dotted lines are eye guide.

The toroidal rotation velocity near the measured point of the reflectometer and the ECE diagnostics is -20±10 km·s^{-1}. Here, minus means the direction counter to the plasma current. Assuming that the precursor frequency is determined by the V_T and the toroidal mode number (n), possible n is evaluated to be 6-17 using the reflectometer signal only. To identify n and V_T, multi-point precursor measurements have been performed using the heterodyne radiometer and the grating polychromator. Since the toroidal separation of these diagnostics is 60 degree, it is impossible to identify larger n than 6 directly. However, the phase delay and the frequency of the precursor in ECE signals can indicate possible combinations of n and V_T taking account of the toroidal separation and the measured V_T. FIG. 3 shows the temperature precursors in three different cases within 0.8 s under the same plasma condition. Although the

relative phase between radiometer and polychromator is changed, it is not due to the change in the direction of the propagation, but due to the aliasing of the measurement because of the large toroidal separation of 60 degrees. Dashed lines in FIG. 3 are simulated signal and the model parameters of n and V_T are determined by adjusting the simulated signal to observed temperature precursors. Observed phase difference in FIG. 3(a)&3(b), 3(c)&3(d) and 3(e)&3(f) can be reproduced with $n = 8 + 6x$, $n = 9 + 6x$ and $n = 10 + 6x$, respectively. Here, x is positive integer depending on V_T. Assuming that the toroidal rotation velocity of the precursor is equal to the edge toroidal rotation speed of -20±10 km·s^{-1}, the dominant mode number of n = 8-10 (V_T ~ -20 km·s^{-1}) or 14-16 (V_T ~ -12 km·s^{-1}) are deduced. It is noted that the dominant mode number varies with ELMs among the range of n (8-10 or 14-16) even in the same plasma conditions. In 28 ELMs for 0.8 s in E49217, 6 ELMs have n = 8 or 14, 3 ELMs have n = 9 or 15 and 8 ELMs have n = 10 or 16 (it is difficult to identify n in other 11 ELMs). The linear MHD stability analysis for E49217 using MARG2D [11] shows that n = 15 mode is unstable and other modes with n = 12-17 are also marginally unstable, suggesting that a small difference in edge plasma conditions determines the dominant n number for each ELM crash.

These experimental results suggest that the precursor phase can be considered as a linear growth phase of peeling-ballooning modes and the instability with such a small growth rate determines the onset condition of type I ELM.

3. Dependence of ELM amplitude on pressure gradient inside pedestal

The dependence of $\Delta W_{ELM}/W_{ped}$ on p'_{in}/p'_{ped} has been investigated using experimental data based on hybrid scenario development in JT-60U [12-13]. The definition of p'_{in} and p'_{ped} can be seen in a small figure in FIG. 5(a). After the calculation of the fast ion component using OFMC code, the pressure gradients inside and within the pedestal are evaluated ($p' = dp/d\rho$, here ρ is normalized minor radius in toroidal flux coordinates). In the dataset, most of the plasma parameters such as plasma shape (R/a = 3.4 m/0.9 m, κ ~ 1.4, δ ~ 0.3), plasma current (I_p = 0.9 MA), toroidal magnetic field (B_T = 1.6 T) and safety factor at 95% flux surface (q_{95} ~ 3.3), are fixed. The variation of p'_{ped} is mainly due to the difference in the heating power (P_{net} = 6.5-9.4 MW) and the different core confinement causes a variation of p'_{in}. In the dataset, the ELM frequency varies between 43-103 Hz depending on the heating power, the plasma density and the recycling.

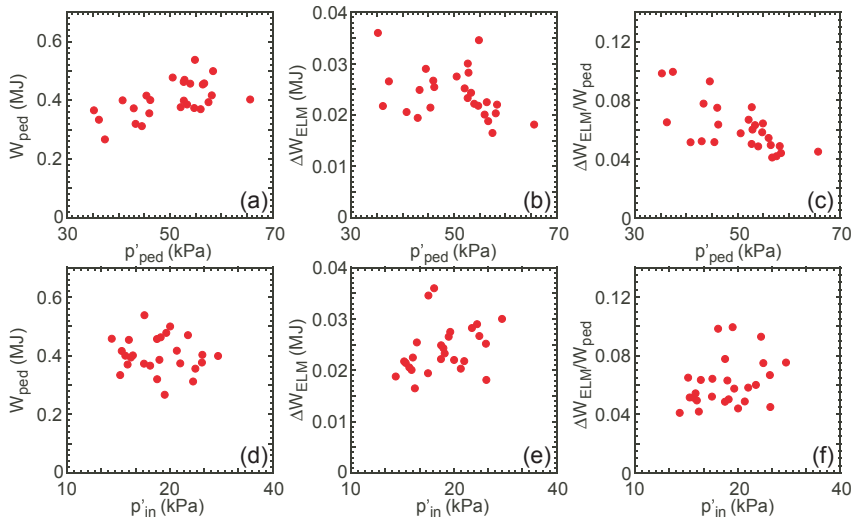

FIG. 4. W_{ped}, ΔW_{ELM} and $\Delta W_{ELM}/W_{ped}$ as a function of p'_{ped} or p'_{in}.

FIG. 4 compares W_{ped}, ΔW_{ELM} and $\Delta W_{ELM}/W_{ped}$ as a function of p'_{ped} or p'_{in}. As can be seen in FIG. 4(a) and 4(b), W_{ped} clearly increases with increasing p'_{ped}, while the dependence of ΔW_{ELM} on p'_{ped} is not so clear. Then, $\Delta W_{ELM}/W_{ped}$ tends to decrease with increasing p'_{ped} as shown in FIG. 4(c). On the other hand,

ΔW_{ELM} tends to increase with p'_{in}, while no dependence of W_{ped} on p'_{in} is observed, as can be seen in FIG. 4(d) and 4(e). However, the data in FIG. 4(f) is scattered and no clear dependence of $\Delta W_{ELM}/W_{ped}$ on p'_{in} can be seen.

Based on the dataset shown in FIG. 4, the dependence of $\Delta W_{ELM}/W_{ped}$ on p'_{in}/p'_{ped} is shown in FIG. 5(a). In contrast to p'_{ped} dependence and p'_{in} dependence shown in FIG. 4(c) and 4(f) respectively, $\Delta W_{ELM}/W_{ped}$ increases linearly with p'_{in}/p'_{ped} as predicted by the integrated ELM modeling using TOPICS-IB code. The dataset shown in FIG. 5(a) is plotted against edge ν_e^* or edge V_T in FIG. 5(b) and 5(c), respectively. In both cases, no clear relation can be seen.

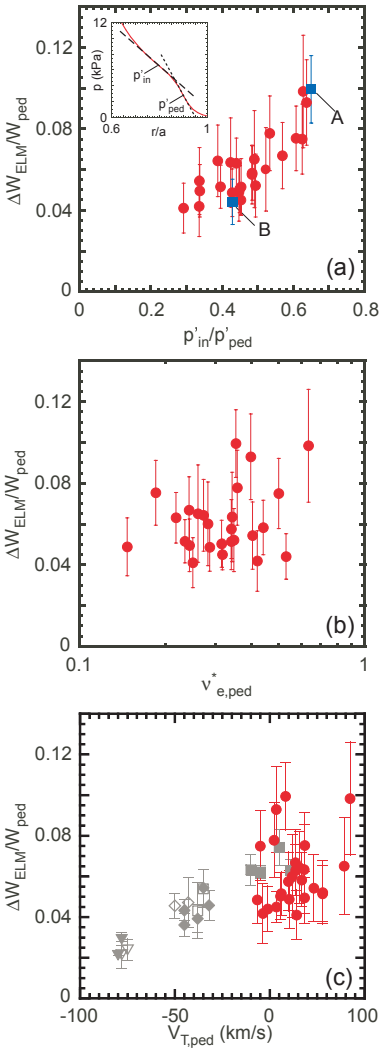

FIG. 5. (a) Normalized ELM energy loss as a function of the ratio of pressure gradient inside (p'_{in}) and within (p'_{ped}) the pedestal. Definition of p'_{in} and p'_{ped} is also plotted in small figure. (b) Normalized ELM energy loss as a function of the edge collisionality. (c) Normalized ELM energy loss as a function of the edge toroidal rotation speed. Gray symbols shows V_T dependence reported in [8].

Changes in the ion temperature profile before and after an ELM, which indicates the ELM affected area, are compared in FIG. 6(a) for the two discharges marked by A and B in FIG. 5(a). The larger reduction rate (amplitude of the ELM) within the pedestal as well as wider ELM affected area is observed in case A. It is noted that W_{ped} in case A is smaller than case B as can be seen in the pressure profiles shown in FIG. 6(b), while larger ΔW_{ELM} is observed (26.6 kJ in case A and 22.1 kJ in case B), resulting larger $\Delta W_{ELM}/W_{ped}$ in case A. Thus, the pressure at the top of the pedestal and its gradient (p'_{ped}) are not main parameter in determining ΔW_{ELM} and $\Delta W_{ELM}/W_{ped}$.

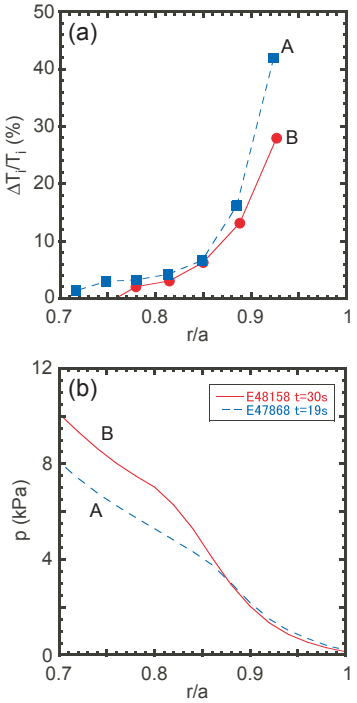

FIG. 6. (a) Comparison of reduction rate of ion temperature profiles for two discharges marked by A and B in FIG. 5(a). (b) Total pressure profiles for two discharges.

In the integrated ELM modeling using TOPICS-IB code [9], the ELM crash is modeled by the increasing particle diffusivity (D) and thermal diffusivity (χ) to 100 m^2s^{-1} for fixed duration of 200 μs. Using this model, larger ΔW_{ELM} is mainly attributed to wider ELM affected area and no large difference in $\Delta T/T$ is predicted. Since the different amplitude of the ELM within the pedestal has been observed in the experiment as shown in FIG. 6(a), new modeling of the maximum value of D and χ during ELM crash will be useful for better prediction.

4. ELM control using edge ECW injection

The effects of local electron heating near the pedestal by the ECW injection on ELM characteristics have been investigated in JT-60U. In order that the ECW power is absorbed near the pedestal in plasmas with I_p = 0.96 MA and B_T = 1.7 T (q_{95} ~ 3.3), the injection angle of the second harmonic X-mode ECW having the frequency of 110 GHz is adjusted as shown in FIG. 7(a). When 1.57 MW of ECW power (injection power is 1.73 MW) is absorbed near the top of the pedestal on high-field side as shown in FIG. 7(b), the ELM frequency increases from 45 Hz to 90 Hz with increasing edge T_e as shown in FIG. 8(a) and 8(b). With this change in the ELM frequency, ΔW_{ELM} is reduced from 31.1 kJ to 20.3 kJ as can be seen in FIG. 8(d), while keeping the W_{ped} almost constant. Shortly after the increase in the edge T_e and the ELM frequency, both core and edge density are gradually reduced by ~7 % taking ~200 ms. The reduction of the total stored energy by ~8 % is mainly attributed to this density pump-out.

After the ECW is stopped, the plasma enters a short ELM free H-mode phase (~65 ms) as shown in FIG. 8(e)-8(h). During this phase, the plasma density and the stored energy recover quickly. At the end of the ELM free phase, higher pedestal pressure can be achieved than that before the ECW injection, which is due to higher pedestal temperature. Then, ELMy H-mode phase with the ELM frequency of 50 Hz, similar to that before ECW injection, is reappeared. After about five ELMs, the pedestal temperature gradually decreases to the same temperature before the ECW injection as shown in FIG. 8(f). These observations suggest that a change in the edge stability due to the edge ECW injection plays an important role in determining the ELM characteristics.

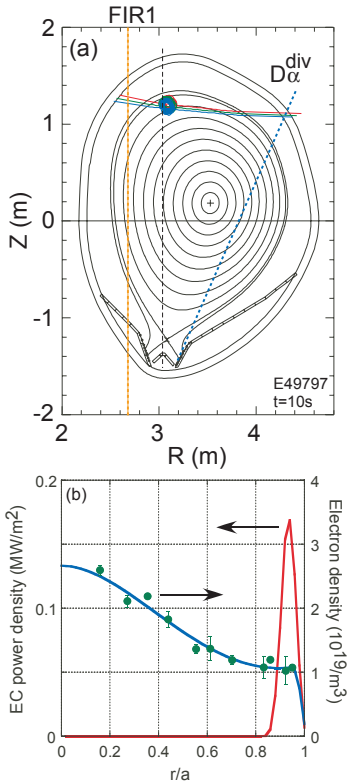

FIG. 7. (a) Plasma configuration for ELM control experiments together with the line of sight of FIR interferometer and D_α intensity (Dotted lines). Dashed line indicates resonant location for second harmonic ECW. Three lines show ray of ECW and absorbed locations. (b) EC power density profile and electron density profile.

The typical characteristic of type I ELM is that the ELM

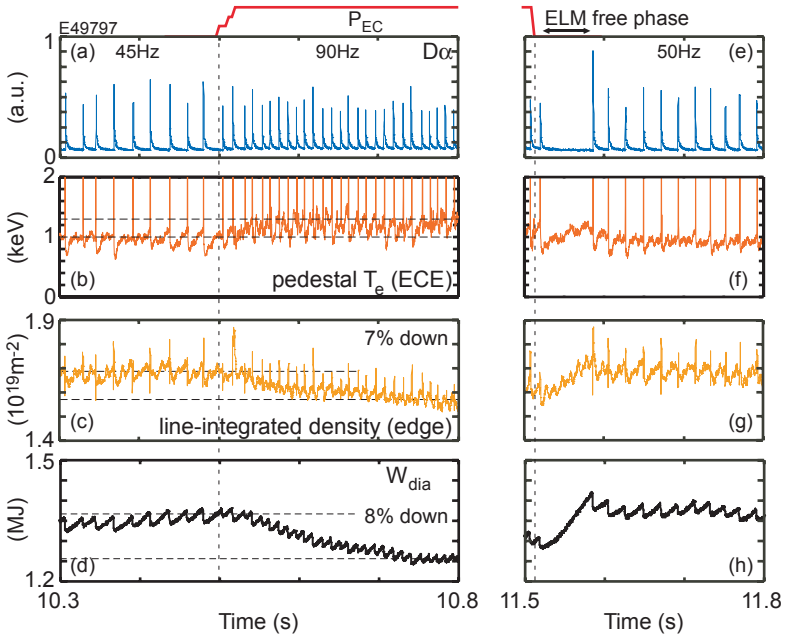

FIG. 8. Waveforms of (a) D_α intensity at outer divertor, (b) electron temperature at pedestal (c) line-integrated density at high-field side edge and (d) stored energy. Time trace of ECW power is also plotted on (a). (e)-(h) waveforms after ECW power is stopped.

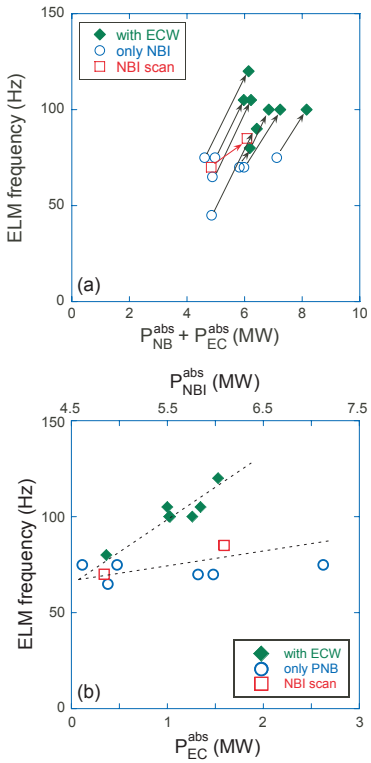

FIG. 9. (a) ELM frequency as a function of total heating power. Absorbed NBI power includes ohmic heating power. (b) ELM frequency as a function of ECW power or incremental NBI power above 4.5 MW. Dotted lines are eye guide.

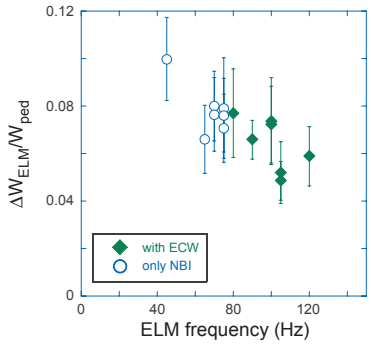

FIG. 10. Normalized ELM energy loss as a function of ELM frequency.

frequency increases with the loss power through the separatrix, which is proportional to the heating power. In order to confirm whether the observed change in the ELM characteristics is due to the power dependence of the type I ELM or not, the ELM frequency as a function of the absorbed power is compared between plasmas with the ECW injection and heated by NBI only as shown in FIG. 9(a). In a wide range of initial heating power of NBI, the increase in the ELM frequency is observed. Even in the high β plasma (β_N = 2.4), the ELM frequency can be increased. It is noted that the increasing rate of the ELM frequency is independent from the initial heating power or the initial ELM frequency. Based on these results, for more direct comparison, FIG. 9(b) shows the ELM frequency as a function of EC power or incremental NBI power above 4.5 MW for plasmas with similar recycling level. As can be seen, the increasing rate with ECW injection is about four times larger than only NBI heating case. In addition, the increase in the injection power of NBI by 2.2 MW (absorbed power of 1.2 MW) only raised the ELM frequency from ~70 Hz to ~85 Hz as shown by squares in FIG. 9. These results indicated that the increase in the ELM frequency with the ECW injection is not due to the increase in the heating power.

In order to understand how effective the ECW injection is to reduce the ELM energy loss, the relation between $\Delta W_{ELM}/W_{ped}$ and the ELM frequency is compared in FIG. 10. The $\Delta W_{ELM}/W_{ped}$ decreases with increasing the ELM frequency. Thus, the localized EC injection near the pedestal can be considered as a candidate for an active ELM control technique in ITER, although the plasma confinement is slightly degraded.

When the ECW is injected into core plasma, well inside the top of the pedestal, the increasing rate of the ELM frequency is similar to the NBI case. Thus, the absorbed location of the ECW seems to be important. When ECW is injected at the top of pedestal on the low-field side in plasmas with I_p = 0.8 MA and B_T = 2.2 T (q_{95} ~ 5.0), no reduction of ΔW_{ELM} has been observed so far. Although 1.6 MW of the ECW power is absorbed with the power deposition profile similar to the high-field side injection case, the ELM frequency decreases from 65 Hz to 55 Hz with increasing ΔW_{ELM}. The different response between high- and low-field side injections implies that the electron cyclotron current drive (ECCD) at edge region may play an important role in the ELM control. Thus, the ECCD profile calculated by Fokker-Planck code [14] is compared with the total edge current profile including the edge bootstrap current. In E49797 shown in FIG. 8, the maximum edge current density of 130 kA·m^{-2} is 16 times larger than the maximum ECCD of 8.3 kA·m^{-2}. It is difficult to change the edge stability by this level of the small

change in the current profile. Therefore, the change in the stability through the modification of the edge current profile may not be a main reason why the ELM characteristics are changed. The understanding the physics mechanism of the ELM control by the edge ECW injection is left for the future work.

5. Summary

The growth rate of the type I ELM precursor in the density fluctuation measured at the outer midplane is systematically evaluated in three different pedestal conditions. The growth rate of the precursor normalized to ω_A is evaluated to be 10^{-3} in all three cases. The phase delay between ECE signals measured at two toroidal locations and the frequency of the precursor indicates n = 8-10 or 14-16 assuming that the precursor rotates toroidally with the same toroidal rotation velocity of carbon impurity. It is noted that the dominant n varies with each ELM under the same plasma condition. The dependence of $\Delta W_{ELM}/W_{ped}$ on p'_{in}/p'_{ped}, which is predicted by integrated ELM modeling using TOPICS-IB code, has been confirmed using experimental data in JT-60U. When the ratio of p'_{in}/p'_{ped} increases from 0.3 to 0.6, $\Delta W_{ELM}/W_{ped}$ increases from 0.04 to 0.10. The dependence can not be explained by either the edge collisionality dependence or the edge toroidal rotation dependence of $\Delta W_{ELM}/W_{ped}$. Therefore, a reliable prediction of the edge pressure profile across the top of the pedestal will be required for a better prediction of the ELM energy loss in ITER. The effects of the local heating near the pedestal by the ECW injection on ELM characteristics have been investigated in JT-60U. When the ECW is injected near the top of the pedestal on high-field side, the $\Delta W_{ELM}/W_{ped}$ can be reduced together with the increase in the ELM frequency. The increasing rate of the ELM frequency with the heating power is four times larger in the ECW injection case than the NBI case, suggesting the localized ECW injection to the edge plasma can be considered as a candidate for an active ELM control technique in ITER.

Acknowledgement

The authors would like to acknowledge all people who have contributed to the JT-60U projects. This research was partly supported by the Grant-in-Aid for Young Scientists (B) 22760666, Japan Society for the Promotion of Science.

References

[1] ZHITLUKHIN, A., et al., J. Nucl. Mater. **363-365** (2007) 301.
[2] LOARTE, A., et al., Plasma Phys. Control. Fusion **45** (2003) 1549.
[3] OYAMA, N., et al., Plasma Phys. Control. Fusion **48** (2006) A171.
[4] OYAMA, N., J. Phys.: Conf. Ser. **123** (2008) 012001.
[5] MAGGI, C.F., Nucl. Fusion **50** (2010) 066001.
[6] OYAMA, N., et al., Nucl. Fusion **44** (2004) 582.
[7] BEURSKENS, M.N.A., Plasma Phys. Control. Fusion **51** (2009) 124051.
[8] URANO, H., et al., Nucl. Fusion **47** (2007) 706.
[9] HAYASHI, N., et al., Nucl. Fusion **49** (2009) 095015.
[10] HORTON, L., et al., Plasma Phys. Control. Fusion **46** (2004) B511.
[11] AIBA, N, et al., Comput. Phys. Commun. **175** (2006) 269.
[12] OYAMA, N., et al., Nucl. Fusion **47** (2007) 689.
[13] OYAMA, N., et al., Nucl. Fusion **49** (2009) 065026.
[14] HAMAMATSU, K., and FUKUYAMA, A., Plasma Phys. Control. Fusion **42** (2000) 1309.